

High-fidelity detection of large-scale atom arrays in an optical lattice

Renhao Tao,^{1,2,3,*} Maximilian Ammenwerth,^{1,2,*} Flavien Gyger,^{1,2,*}
Immanuel Bloch,^{1,2,3} and Johannes Zeiher^{1,2,3,†}

¹*Max-Planck-Institut für Quantenoptik, 85748 Garching, Germany*

²*Munich Center for Quantum Science and Technology (MCQST), 80799 Munich, Germany*

³*Fakultät für Physik, Ludwig-Maximilians-Universität, 80799 Munich, Germany*

(Dated: April 29, 2024)

Recent advances in quantum simulation based on neutral atoms have largely benefited from high-resolution, single-atom sensitive imaging techniques. A variety of approaches have been developed to achieve such local detection of atoms in optical lattices or optical tweezers. For alkaline-earth and alkaline-earth-like atoms, the presence of narrow optical transitions opens up the possibility of performing novel types of Sisyphus cooling, where the cooling mechanism originates from the capability to spatially resolve the differential optical level shifts in the trap potential. Up to now, it has been an open question whether high-fidelity imaging could be achieved in a “repulsive Sisyphus” configuration, where the trap depth of the ground state exceeds that of the excited state involved in cooling. Here, we demonstrate high-fidelity (99.971(1)%) and high-survival (99.80(5)%) imaging of strontium atoms using repulsive Sisyphus cooling. We use an optical lattice as a pinning potential for atoms in a large-scale tweezer array with up to 399 tweezers and show repeated, high-fidelity lattice-tweezer-lattice transfers. We furthermore demonstrate loading the lattice with approximately 10000 atoms directly from the MOT and scalable imaging over > 10000 lattice sites with a combined survival probability and classification fidelity better than 99.2%. Our lattice thus serves as a locally addressable and sortable reservoir for continuous refilling of optical tweezer arrays in the future.

Laser-cooled atomic gases trapped in optical lattices have enabled a number of breakthroughs in quantum sciences [1–3]. An entirely new level of control of such systems was reached by the development of quantum-gas microscopes [4, 5]. These setups have enabled single-site- and single-atom-resolved detection of atomic many-body systems in a top-down approach starting from a quantum-degenerate gas prepared via evaporative cooling. A prerequisite to quantum-gas microscopy is the high-fidelity and low-loss imaging of atoms in optical lattices. For alkali atoms, cooling during imaging can be achieved either by polarization gradient cooling [4, 5] or Raman sideband cooling [6–8]. In alkaline-earth and alkaline-earth-like atoms, the presence of a narrow optical intercombination transition opens up the perspective for new, efficient cooling strategies [9–13]. In particular, high-resolution imaging of atoms in optical lattices has been achieved for ytterbium atoms [14], and recently for strontium atoms in a clock-magic optical lattice at 813 nm [15–17].

Atom assembly in arrays of optical tweezers provides an alternative, bottom-up approach for the study of many-body systems with single-atom preparation, control and detection capabilities [18–20]. This approach benefits from the re-configurable design of array patterns in various dimensions [21–23], as well as the ability of single-site addressing and atom positioning [22–24]. These features have resulted in successful implementations of tweezer arrays in various fields such as quantum metrology [25–27], quantum computing [24, 28–

33] and quantum simulation [34, 35]. While bottom-up and top-down approaches have been developed mostly in parallel, increasing efforts have recently been undertaken to combine both platforms, leading to novel ways of preparing atoms in optical lattices in the Hubbard regime [16, 17, 36], coupling freely configurable optical tweezer arrays for realizing Hubbard models [37, 38] or creating novel programmable optical lattice potentials via selective blocking of specific sites in optical lattices [39]. This hybrid approach has also played a role in scaling neutral-atom systems by allowing optimal use of different potentials for distinct experimental stages, for instance, in creating programmable arrays of ~ 100 optical qubits in magic wavelength potentials [15, 40].

Here, we demonstrate preparation and detection of 10^4 single atoms using a hybrid lattice-tweezer platform. This significant advance in system size for the field of atomic arrays is enabled by several innovations going beyond previous work. In particular, employing a specially purposed trapping geometry and a previously unexplored lattice trapping wavelength for strontium atoms at 1040 nm, we demonstrate high-fidelity, low-loss detection of the atoms in the optical lattice. We quantify the imaging performance in this novel configuration and report a classification fidelity exceeding 99.9% combined with a survival probability exceeding 99.29(1)% averaged over 10450 sites of the lattice. Our work surpasses the state of the art in demonstrating the largest number of traps amenable to high-fidelity and low-loss imaging to date [17, 35, 41]. We furthermore show that a dense cloud of atoms can be directly loaded into a single plane of the lattice from a magneto-optical trap, and subsequently imaged with high fidelity and low loss, opening the path to an entirely different approach to scaling atom arrays. In

* These authors contribute equally to this work.

† johannes.zeiher@mpq.mpg.de

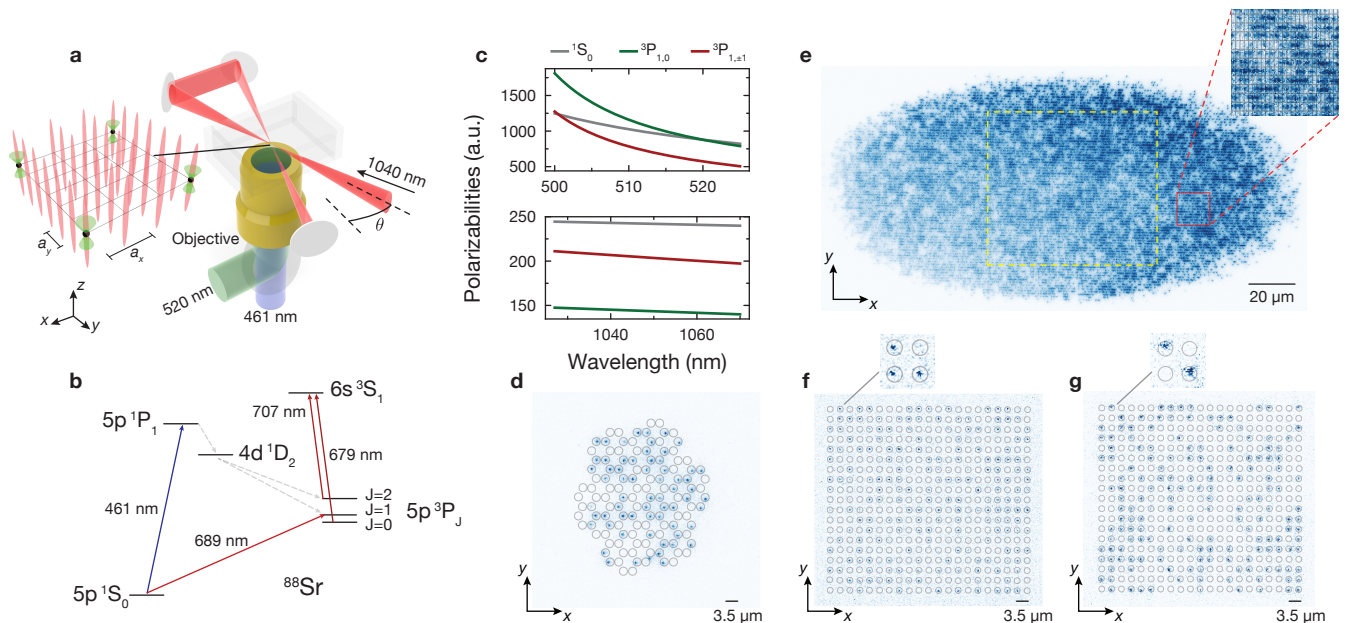


FIG. 1. Experimental setup. **a** An optical lattice is formed from a single elliptical beam at wavelength 1040 nm retro-reflected in the xy plane. At the crossing angle $\theta = 26^\circ$, the lattice spacing is $a_x = 579(2)$ nm along the x -axis and $a_y = 1187(18)$ nm along the y -axis. The tweezer array (green) is created with a spatial light modulator (SLM) and light at wavelength 520 nm. The tweezers are focused into the glass cell and overlapped with lattice sites in 3D (inset). The fluorescence of atoms is collected by the objective and separated from the tweezer light with a dichroic. **b** Level diagram for transitions involved in this work. We resonantly scatter photons on the 1S_0 - 1P_1 transition (461 nm), while simultaneously cooling on the 1S_0 - 3P_1 transition (689 nm). Atoms leaking out of the imaging cycle are repumped via transitions at 679 nm and 707 nm. **c** Calculated polarizabilities of 1S_0 and $^3P_{1,m_J}$ at green tweezer wavelengths (upper panel) and infrared lattice wavelengths (lower panel). At trapping wavelengths ranging from 500 to 520 nm, 1S_0 - $^3P_{1,m_J=0}$ can be made magic via mixing of the polarizabilities for different Zeeman sublevels under strong magnetic field [9]. The mixing ratio can be tuned via the angle ϕ between the bias field and the linear tweezer polarization. At 1040 nm, cooling on the narrow line occurs in the repulsive Sisyphus regime. **d** Typical single-shot image of atoms loaded from a honeycomb-shaped tweezer array and imaged in the lattice. Circles denote the programmed tweezer location. **e** A single-shot image of more than 10000 single atoms directly loaded into the lattice from the magneto-optical trap. The yellow dashed box denotes the spatial extent of the tweezer array used in this work. The smaller red box is a zoom-in which shows well-resolved single atoms. **f** Typical single-shot image of a 21×19 tweezer array imaged directly in 520 nm tweezer. The tweezer spacing is $3.478(1)(3.549(1)) \mu\text{m}$ along the $x(y)$ -axis which is precisely chosen to be $6a_y(3a_x)$, respectively. **g** Typical single-shot image of atoms loaded from a tweezer array into the lattice and imaged there. Due to weaker axial (z -axis) confinement, the point-spread function of atoms imaged in the lattice is about 1.7 times larger than that in tweezers.

addition, we demonstrate repeated handover between the lattice and tweezers generated using a spatial light modulator (SLM), and reinitialization of the tweezer-trapped atoms in low-temperature states after the imaging step in the lattice. Finally, our results settle an ongoing discussion raised by earlier work [10, 42, 43] on whether repulsive Sisyphus cooling and high-fidelity and low-loss imaging are compatible.

In our experiment, we combine an optical tweezer array comprising 399 optical traps at wavelength $\lambda_{tw} = 520$ nm and an optical lattice operated at wavelength $\lambda_l = 1040$ nm, see Fig. 1a. Using computer-generated holograms, we routinely create tweezer arrays with trap spacings of $3.478(1)(3.549(1)) \mu\text{m}$ along the $x(y)$ -axis and waists of $473(3)$ nm, with excellent control over positioning, spacing and arrangement of the individual traps, see [44]. The optical lattice is formed in a bow-tie

configuration [45], where a single beam creates a two-dimensional lattice potential by four-fold interference. In addition, we tightly focus the lattice in the z -axis to a waist of $20 \mu\text{m}$, which provides a vertical confinement of up to 5.9 kHz at a lattice depth of 1.47 mK. The half-angle θ is about 26° chosen to have lattice constants ratio of 1:2 along two axes. In this configuration, the radial trap frequencies are 150 kHz and 300 kHz respectively, such that we achieve complete 3D confinement using a single lattice beam only. Cooling in the various configurations described above is performed with a single beam addressing the 1S_0 - 3P_1 transition at 689 nm, see Fig. 1b. For imaging, we additionally illuminate the atoms with light at 461 nm, which induces fluorescence on the broad 1S_0 - 1P_1 transition. We collect the fluorescence photons with the same objective that is used to generate the tweezer array with a specified $\text{NA} = 0.65$.

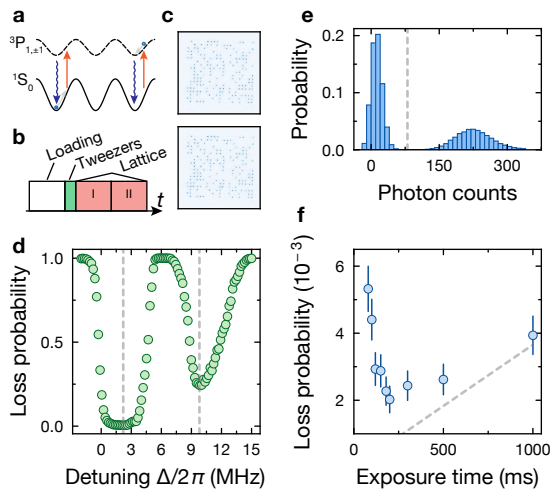


FIG. 2. **Imaging in the lattice.** **a** Illustration of repulsive Sisyphus cooling dynamics for 1S_0 and $^3P_{1,\pm 1}$ states in the lattice. **b** Schematic of experimental sequence for imaging in the lattice. Two images (I & II) in the lattice are taken after atoms are prepared in tweezers and transferred into the lattice. Loss probability is calculated by comparing occupations between image I and II. **c** Exemplary consecutive fluorescence images of individual atoms in the lattice showing no loss. **d** Array-averaged atom loss probability as a function of 689 nm cooling laser detuning Δ from the 1S_0 - 3P_1 resonance in free space for an imaging exposure time of 300 ms. At $\Delta/2\pi = 2.2$ MHz, imaging loss reduces down to 2×10^{-3} . **e** Array-averaged histogram of photon counts taken with exposure time 300 ms, showing a well-resolved background and one-atom fluorescence peak. The classification fidelity can be as high as 99.971(1)%, see [44]. **f** Imaging loss at constant scattered photon number for classification infidelity of 10^{-4} vs. exposure time. The lower dashed gray line indicates atom loss probability attributed to our estimated vacuum lifetime of 273(3) s, which is reached by our imaging in the limit of long exposure time and low illumination power. The background level remains similarly low all all exposure times.

This has allowed us to resolve atoms spaced as closely as one lattice site $a_x = 579(2)$ nm, see Fig. 1.

As a first step, we demonstrate high-fidelity and low-loss imaging in a repulsive Sisyphus regime. This is relevant for strontium at our lattice wavelength of 1040 nm, where $\omega_g/\omega_e = 1.08$ for the $^3P_{1,m_J=\pm 1}$ as the excited state, see Fig. 2a. We begin the experiment with an array of atoms at 399 singly-occupied lattice sites loaded from tweezers, see [44]. To optimize the cooling performance for imaging, we scan the detuning Δ of the cooling light relative to the free-space resonance, see Fig. 2d. We obtain a broad cooling feature at approximately 2.2 MHz, where the atom loss fraction reaches the sub-percent, and a second narrower feature at about 9.8 MHz, where the loss is higher. The two features can be attributed to cooling on 1S_0 - $^3P_{1,m_J=\pm 1}$ and 1S_0 - $^3P_{1,m_J=0}$ respectively and are consistent with the 689 nm transition split by tensor lightshift in the 1040 nm lattice. To characterize imaging performance under cooling on the $m_J = \pm 1$

transition, we take two consecutive images in the optical lattice, see Fig. 2c. The images are binarized based on the tweezer-averaged histogram of the integrated photon count, see Fig. 2e. With an optimal threshold [44], we obtain a classification infidelity of approximately 10^{-4} , demonstrating the feasibility of high-fidelity imaging in our lattice. To benchmark the atom loss probability from imaging, we compare the occupation of the two consecutively acquired images as a function of the exposure time, see Fig. 2f. For this measurement, we keep the integrated photon number scattered on the 461 nm transition and hence the classification fidelity constant. We find a robust minimum atom loss probability at an exposure time of approximately 200 ms, where the loss reaches 2×10^{-3} . At shorter exposure times and hence larger imaging beam scattering rate, the atom loss probability increases as a result of recoil heating exceeding the cooling rate from Sisyphus cooling. For longer exposure times, the atom loss probability begins to be dominated by our estimated vacuum lifetime of 273(3) s.

The feasibility of high-fidelity, low-loss imaging in the lattice offers the perspective of decoupling the power-intensive imaging step from cooling and physics performed in optical tweezers, provided efficient transfer between lattice and tweezer array. Such a capability would allow for the use of advantageous features of tweezers at 520 nm, e.g. for trapping of Rydberg states via the ionic core polarizability [46], while avoiding lossy detection at the same wavelength [10, 43]. We characterize the lattice-tweezer transfer via the round-trip atom loss probability after imaging first in the lattice, see Fig. 3a. A challenge in this case is the weak vertical confinement of our 2D lattice, whose waist in the z -direction significantly exceeds the Rayleigh range of $1.5 \mu\text{m}$ of the tweezers, see Fig. 3a. To enable low-loss transfer back to tweezers, we first perform an optimized repulsive Sisyphus cooling in the lattice after imaging (II). Subsequently, we ramp up the tweezers to a depth of $300 \mu\text{K}$, before lowering the lattice to an intermediate depth of $150 \mu\text{K}$. We perform a second stage of cooling in this combined potential to efficiently transfer the atoms into trapped states in the tweezers. The cooling frequency is chosen to coincide with the lattice-light shifted cooling sideband of the tweezers and the magnetic field is set to the magic cooling transition in tweezers alone [44]. Finally, we ramp the lattices down in 50 ms, completing the transfer to the tweezers. Imaging is then performed once more in the lattice, with an identical tweezer-lattice handover as before the first image. We benchmark the complete round-trip atom loss probability p_n by comparing the reconstructed tweezer occupation between two images taken in the lattice before and after n transfers, see Fig. 3c. While the overall atom loss probability increases with the number of round-trips as expected, we find that the atom loss probability per round-trip p_1 , extracted under the assumption of a simple power-law scaling of the atom loss probability $1 - p_n = (1 - p_1)^n$, continuously decreases from 1.3% down to approximately 5×10^{-3} after a few round-trips.

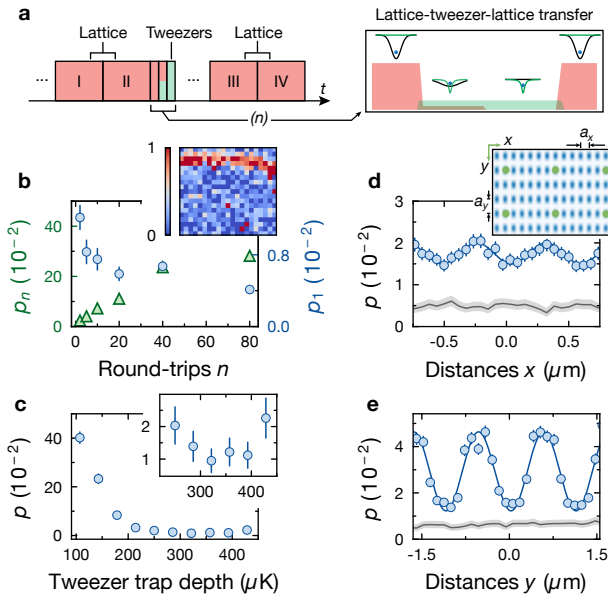


FIG. 3. **Transfer between lattice and tweezers.** **a** Schematic of experimental sequence for tweezer-lattice-tweezer transfers. Axial potential landscape of the tweezers (green) and lattice (black) during hand-over is shown in the inset. The sketch is not to scale. **b** Cumulative loss probability p_n (blue round markers) of atoms versus the number of lattice-tweezers-lattice round-trips n . The average single round-trip atom loss probability p_1 (green triangles) decreases as n increases. The atom loss probability p_n shows a pronounced spatial dependence predominantly at the boundary of the lattice, as apparent from a measurement of the site-resolved atom loss probability after $n = 80$ round-trips (inset). **c** Single-round-trip atom loss probability p as function of tweezer trap depth after transfer. The inset shows a close-up and confirms tweezer averaged single-round-trip losses close to 1%. **d,e** Single-round-trip atom loss probability p vs. relative position between lattice and tweezer potentials along x -axis (**d**) and y -axis (**e**) shown as blue points. The sinusoidal fit reflects the expected lattice potential with a lattice constant $a_x = 579(2)$ nm and $a_y = 1187(18)$ nm. The atom loss probability due to imaging alone is indicated by shaded gray lines. Inset: Sketch of the tweezer traps (green dots) and the lattice potential (blue dots).

We attribute the initially higher atom loss probability predominantly to a systematic spatial inhomogeneity affecting our cooling in the lattice during transfer, which becomes directly apparent in a tweezer-resolved transfer loss map after $n = 80$ round-trips, see Fig. 3b inset. Hence, we consider the reported transfer loss as a worst case scenario that can be improved by excluding the traps exhibiting high atom loss or centering the tweezer array in the lattice. We find that highly efficient transfers are possible if the tweezer depth in the transfer exceeds approximately $300 \mu\text{K}$, see Fig. 3c. For the last point beyond $400 \mu\text{K}$, the transfer loss probability increases slightly due to non-optimal cooling parameters. To study the dependence of the transfer efficiency on the

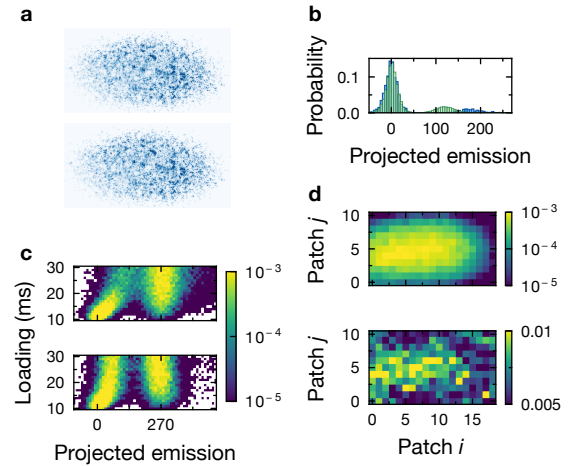


FIG. 4. **Imaging characterization over the entire lattice loaded directly from the MOT** **a** We load the lattice directly from the MOT and take two consecutive images to characterize the imaging performance over a much larger region of the lattice. The sparse filling gives rise to a higher classification fidelity (see discussion below) and aids in the bench-marking. **b** Coarse-grained histograms of two representative lattice patches (10×5 sites) show the spread of the emissions due to fluorescence inhomogeneity. **c** The detected counts versus MOT loading time for two consecutive images reveals the parity projection for an exposure time of 1.8 s, signalled by the absence of the tail of the histograms extending into high emission counts at large loading times in the second image. The double-occupancy accounts for less than 0.3% of all emissions events at 30 ms loading time. **d** Coarse-grained classification infidelity (upper panel) analyzed on individual patches in the entire lattice. The classification error is below 10^{-3} . The higher infidelity at the lattice center correlates well to the atom density, as a result of cross-talk that worsens at higher lattice filling fraction. The coarse-grained loss probability (lower panel) of two consecutive images demonstrates that the imaging loss computed from consecutive images is as low as $7.1(1) \times 10^{-3}$. To further optimize the performance, the exposure time was set to 900 ms for this measurement.

relative position between lattice sites and tweezers, we scan the position of the tweezer array along either the x - or y -axis, see Fig. 3d, e. We find a pronounced sinusoidal dependence of the transfer loss, which reaches up to 5% in non-optimal conditions. Close to the optimal condition, we obtain a $\sim 90\%$ fidelity of finding an atom at exactly the same lattice sites before (II) and after (III) holding them in the tweezers. The observed sinusoidal structure is in excellent agreement with the expected dependence for our lattice, and the curves represent a characterization of the underlying lattice structure using a large-scale tweezer array [47]. We note that even after imaging in the lattice, one can re-cool atoms in tweezers close to the radial motional ground state after transfer them back [44].

To highlight the scalability of our platform, we directly load the lattice from the MOT for variable durations and characterize the imaging performance for the loaded atoms over two consecutive images, see Fig 4a. Impro-

tantly, our lattice configuration renders further single-plane preparation steps before detecting the atomic distribution unnecessary. To benchmark the detection, we binarize the images using deconvolution techniques, which also yields the classification fidelity, see [44]. We evaluate the histogram of recorded photon counts locally, over small patches of 10×5 sites to mitigate the effect of inhomogeneities, see Fig 4b. With increasing loading time, a single-atom peak in the histogram of the first acquired image develops at 270 photon counts, corresponding to the amount of photons collected within the exposure time for each singly-loaded site, see Fig 4c. At even longer loading time exceeding 30 ms, a tail beyond 270 counts appears to extend into higher emission counts, which is expected for loading multiple atoms per site. In the second image, this tail is absent even at long loading times, indicating efficient parity projection during the imaging process. To quantify the achieved performance, we characterize the classification fidelity and survival probability in a region of 10450 lattice sites. The coarse-grained analysis indicates that the high lattice filling and consequently cross-talk between sites is the main factor that reduces classification fidelity at long loading time, see Fig 4d. In particular, the higher classification infidelity can be attributed to an increasing width of the zero-atom peak due to the empty sites receiving fluorescence emanating from adjacent occupied sites. Nevertheless, we find that classification infidelity is globally below 10^{-3} for a filling fraction ~ 0.2 which amounts to ~ 2300 loaded atoms. Similarly, the imaging loss is kept at $7.1(1) \times 10^{-3}$, see Fig 4d. The preparation and high-fidelity detection of individual atoms in a single layer of an optical lattice allows for subsequent resorting in the lattice as demonstrated recently in the same setup [48]. Such sorted arrays can then be transferred into tweezer potentials, resulting in a direct two-fold reduction of the required tweezer power due to then deterministic loading of the tweezer array with near unity-filling. Using additional vertical confinement in the transfer allows for significantly relaxed power requirements of the tweezer array, promising further gains in the scalability of tweezer arrays through deterministic loading via optical lattices.

In conclusion, we have demonstrated the feasibility of low-loss and high-fidelity imaging under repulsive Sisyphus cooling conditions on the narrow-linewidth transition of strontium in an optical lattice. We extend the size of the system compatible with single-site and single atom detection to more than 10000 lattice sites and load

more than 10000 atoms directly from the MOT. Our results offer a new path to assembling large atom arrays in optical lattices that clearly surpass the state of the art with respect to the achieved atom numbers in sortable optical tweezers and lattices [17, 35, 41]. Straightforward upgrades of the laser power used in our setup via commercially available off-the-shelf laser systems allow to scale the number of sites by a factor of 10, as a direct consequence of our proof-of-concept demonstration of high imaging quality at 1040 nm, where such laser systems are readily available. Furthermore, our work offers the perspective to operate tweezer arrays at arbitrary wavelengths by decoupling the power-intensive imaging step from preparation and physics in optical tweezer arrays, with potential applications in quantum simulation of Ising models [34, 35, 49, 50], lattice gauge theories [51], quantum chemistry [52], or quantum-enhanced metrology [15, 40, 53, 54] in scalable ensembles. Finally, directly loading the optical lattice from a magneto-optical trap in combination with high-fidelity imaging, resorting and laser-cooling, provides a new bottom-up approach of assembling large-scale Hubbard simulators [16, 17].

ACKNOWLEDGMENTS

We thank Sylvain de Léséleuc and Stepan Snigirev for insightful discussions on tweezer arrays, Isabella Fritsche and the planqc team for help in setting up a high-power tweezer laser setup, Elias Trapp for support in the lab, and David Wei for providing the code for lattice reconstruction. We acknowledge funding by the Max Planck Society (MPG) the Deutsche Forschungsgemeinschaft (DFG, German Research Foundation) under Germany's Excellence Strategy–EXC-2111–390814868, and from the Munich Quantum Valley initiative as part of the High-Tech Agenda Plus of the Bavarian State Government. This publication has also received funding under Horizon Europe programme HORIZON-CL4-2022-QUANTUM-02-SGA via the project 101113690 (PASQuanS2.1). J.Z. acknowledges support from the BMBF through the program “Quantum technologies - from basic research to market” (Grant No. 13N16265). F.G. acknowledges funding from the Swiss National Fonds (Fund Nr P500PT.203162). M.A. and R.T. acknowledge funding from the International Max Planck Research School (IMPRS) for Quantum Science and Technology. M.A. acknowledges support through a fellowship from the Hector Fellow Academy.

[1] C. Gross and I. Bloch, Quantum simulations with ultracold atoms in optical lattices, *Science* **357**, 995 (2017).
 [2] M. Morgado and S. Whitlock, Quantum simulation and computing with Rydberg-interacting qubits, *AVS Quantum Sci.* **3**, 023501 (2021).
 [3] H. Katori, Optical lattice clocks and quantum metrology,

Nat. Photonics **5**, 203 (2011).
 [4] W. S. Bakr, J. I. Gillen, A. Peng, S. Fölling, and M. Greiner, A quantum gas microscope for detecting single atoms in a Hubbard-regime optical lattice, *Nature* **462**, 74 (2009).
 [5] J. F. Sherson, C. Weitenberg, M. Endres, M. Cheneau,

- I. Bloch, and S. Kuhr, Single-atom-resolved fluorescence imaging of an atomic Mott insulator, *Nature* **467**, 68 (2010).
- [6] E. Haller, J. Hudson, A. Kelly, D. A. Cotta, B. Peaudecerf, G. D. Bruce, and S. Kuhr, Single-atom imaging of fermions in a quantum-gas microscope, *Nat. Phys.* **11**, 738 (2015).
- [7] L. W. Cheuk, M. A. Nichols, M. Okan, T. Gersdorf, V. V. Ramasesh, W. S. Bakr, T. Lompe, and M. W. Zwierlein, Quantum-Gas Microscope for Fermionic Atoms, *Phys. Rev. Lett.* **114**, 193001 (2015).
- [8] A. Omran, M. Boll, T. A. Hilker, K. Kleinlein, G. Salomon, I. Bloch, and C. Gross, Microscopic Observation of Pauli Blocking in Degenerate Fermionic Lattice Gases, *Phys. Rev. Lett.* **115**, 263001 (2015).
- [9] M. A. Norcia, A. W. Young, and A. M. Kaufman, Microscopic Control and Detection of Ultracold Strontium in Optical-Tweezer Arrays, *Phys. Rev. X* **8**, 041054 (2018).
- [10] A. Cooper, J. P. Covey, I. S. Madjarov, S. G. Porsev, M. S. Safronova, and M. Endres, Alkaline-Earth Atoms in Optical Tweezers, *Phys. Rev. X* **8**, 041055 (2018).
- [11] J. P. Covey, I. S. Madjarov, A. Cooper, and M. Endres, 2000-Times Repeated Imaging of Strontium Atoms in Clock-Magic Tweezer Arrays, *Phys. Rev. Lett.* **122**, 173201 (2019).
- [12] S. Saskin, J. T. Wilson, B. Grinkemeyer, and J. D. Thompson, Narrow-line cooling and imaging of ytterbium atoms in an optical tweezer array, *Physical Review Letters* **122**, 143002 (2019).
- [13] A. Urech, I. H. A. Knottnerus, R. J. C. Spreeuw, and F. Schreck, Narrow-line imaging of single strontium atoms in shallow optical tweezers, *Phys. Rev. Res.* **4**, 023245 (2022).
- [14] R. Yamamoto, J. Kobayashi, T. Kuno, K. Kato, and Y. Takahashi, An ytterbium quantum gas microscope with narrow-line laser cooling, *New. J. Phys.* **18**, 023016 (2016).
- [15] N. Schine, A. W. Young, W. J. Eckner, M. J. Martin, and A. M. Kaufman, Long-lived Bell states in an array of optical clock qubits, *Nat. Phys.* **18**, 1067 (2022).
- [16] A. W. Young, W. J. Eckner, N. Schine, A. M. Childs, and A. M. Kaufman, Tweezer-programmable 2D quantum walks in a Hubbard-regime lattice, *Science* **377**, 885 (2022).
- [17] A. W. Young, S. Geller, W. J. Eckner, N. Schine, S. Glancy, E. Knill, and A. M. Kaufman, An atomic boson sampler, [arXiv:2307.06936](https://arxiv.org/abs/2307.06936) (2023).
- [18] N. Schlosser, G. Reymond, I. Protsenko, and P. Grangier, Sub-poissonian loading of single atoms in a microscopic dipole trap, *Nature* **411**, 1024 (2001).
- [19] T. Grunzweig, A. Hilliard, M. McGovern, and M. Andersen, Near-deterministic preparation of a single atom in an optical microtrap, *Nat. Phys.* **6**, 951 (2010).
- [20] A. M. Kaufman and K.-K. Ni, Quantum science with optical tweezer arrays of ultracold atoms and molecules, *Nat. Phys.* **17**, 1324 (2021).
- [21] M. Endres, H. Bernien, A. Keesling, H. Levine, E. R. Anschuetz, A. Krajenbrink, C. Senko, V. Vuletic, M. Greiner, and M. D. Lukin, Atom-by-atom assembly of defect-free one-dimensional cold atom arrays, *Science* **354**, 1024 (2016).
- [22] D. Barredo, S. de Léséleuc, V. Lienhard, T. Lahaye, and A. Browaeys, An atom-by-atom assembler of defect-free arbitrary two-dimensional atomic arrays, *Science* **354**, 1021 (2016).
- [23] D. Barredo, V. Lienhard, S. de Léséleuc, T. Lahaye, and A. Browaeys, Synthetic three-dimensional atomic structures assembled atom by atom, *Nature* **561**, 79 (2018).
- [24] D. Bluvstein, H. Levine, G. Semeghini, T. T. Wang, S. Ebadi, M. Kalinowski, A. Keesling, N. Maskara, H. Pichler, M. Greiner, V. Vuletić, and M. D. Lukin, A quantum processor based on coherent transport of entangled atom arrays, *Nature* **604**, 451 (2022).
- [25] I. S. Madjarov, A. Cooper, A. L. Shaw, J. P. Covey, V. Schkolnik, T. H. Yoon, J. R. Williams, and M. Endres, An Atomic-Array Optical Clock with Single-Atom Readout, *Phys. Rev. X* **9**, 041052 (2019).
- [26] M. A. Norcia, A. W. Young, W. J. Eckner, E. Oelker, J. Ye, and A. M. Kaufman, Seconds-scale coherence on an optical clock transition in a tweezer array, *Science* **366**, 93 (2019).
- [27] A. W. Young, W. J. Eckner, W. R. Milner, D. Kedar, M. A. Norcia, E. Oelker, N. Schine, J. Ye, and A. M. Kaufman, Half-minute-scale atomic coherence and high relative stability in a tweezer clock, *Nature* **588**, 408 (2020).
- [28] H. Levine, A. Keesling, G. Semeghini, A. Omran, T. T. Wang, S. Ebadi, H. Bernien, M. Greiner, V. Vuletic, H. Pichler, and M. D. Lukin, Parallel Implementation of High-Fidelity Multiqubit Gates with Neutral Atoms, *Phys. Rev. Lett.* **123**, 170503 (2019).
- [29] T. M. Graham, Y. Song, J. Scott, C. Poole, L. Phuttitarn, K. Jooya, P. Eichler, X. Jiang, A. Marra, B. Grinkemeyer, M. Kwon, M. Ebert, J. Cherek, M. T. Lichtman, M. Gillette, J. Gilbert, D. Bowman, T. Ballance, C. Campbell, E. D. Dahl, O. Crawford, N. S. Blunt, B. Rogers, T. Noel, and M. Saffman, Multi-qubit entanglement and algorithms on a neutral-atom quantum computer, *Nature* **604**, 457 (2022).
- [30] A. Jenkins, J. W. Lis, A. Senoo, W. F. McGrew, and A. M. Kaufman, Ytterbium Nuclear-Spin Qubits in an Optical Tweezer Array, *Phys. Rev. X* **12**, 021027 (2022).
- [31] S. Ma, A. P. Burgers, G. Liu, J. Wilson, B. Zhang, and J. D. Thompson, Universal Gate Operations on Nuclear Spin Qubits in an Optical Tweezer Array of ^{171}Yb Atoms, *Phys. Rev. X* **12**, 021028 (2022).
- [32] S. Ma, G. Liu, P. Peng, B. Zhang, S. Jandura, J. Claes, A. P. Burgers, G. Pupillo, S. Puri, and J. D. Thompson, High-fidelity gates with mid-circuit erasure conversion in a metastable neutral atom qubit, [arXiv:2305.05493](https://arxiv.org/abs/2305.05493) 10.48550/arXiv.2305.05493 (2023).
- [33] S. J. Evered, D. Bluvstein, M. Kalinowski, S. Ebadi, T. Manovitz, H. Zhou, S. H. Li, A. A. Geim, T. T. Wang, N. Maskara, H. Levine, G. Semeghini, M. Greiner, V. Vuletic, and M. D. Lukin, High-fidelity parallel entangling gates on a neutral atom quantum computer, [arXiv:2304.05420](https://arxiv.org/abs/2304.05420) (2023).
- [34] P. Scholl, M. Schuler, H. J. Williams, A. A. Eberharter, D. Barredo, K.-N. Schymik, V. Lienhard, L.-P. Henry, T. C. Lang, T. Lahaye, A. M. Läuchli, and A. Browaeys, Quantum simulation of 2D antiferromagnets with hundreds of Rydberg atoms, *Nature* **595**, 233 (2021).
- [35] S. Ebadi, T. T. Wang, H. Levine, A. Keesling, G. Semeghini, A. Omran, D. Bluvstein, R. Samajdar, H. Pichler, W. W. Ho, S. Choi, S. Sachdev, M. Greiner, V. Vuletić, and M. D. Lukin, Quantum phases of matter on a 256-atom programmable quantum simulator, *Nature* **595**, 227 (2021).

- [36] J. Trisnadi, M. Zhang, L. Weiss, and C. Chin, Design and construction of a quantum matter synthesizer, *Rev. Sci. Instrum.* **93**, 10.1063/5.0100088 (2022).
- [37] S. Murmann, A. Bergschneider, V. M. Klinkhamer, G. Zürn, T. Lompe, and S. Jochim, Two Fermions in a Double Well: Exploring a Fundamental Building Block of the Hubbard Model, *Phys. Rev. Lett.* **114**, 080402 (2015).
- [38] B. M. Spar, E. Guardado-Sanchez, S. Chi, Z. Z. Yan, and W. S. Bakr, Realization of a Fermi-Hubbard Optical Tweezer Array, *Phys. Rev. Lett.* **128**, 223202 (2022).
- [39] D. Wei, D. Adler, K. Srakaew, S. Agrawal, P. Weckesser, I. Bloch, and J. Zeiher, Observation of Brane Parity Order in Programmable Optical Lattices, *Phys. Rev. X* **13**, 021042 (2023).
- [40] W. J. Eckner, N. Darkwah Oppong, A. Cao, A. W. Young, W. R. Milner, J. M. Robinson, J. Ye, and A. M. Kaufman, Realizing spin squeezing with Rydberg interactions in an optical clock, *Nature* 10.1038/s41586-023-06360-6 (2023).
- [41] L. Pause, L. Sturm, M. Mittenbühler, S. Amann, T. Preuschoff, D. Schäffner, M. Schlosser, and G. Birkl, Supercharged two-dimensional tweezer array with more than 1000 atomic qubits, arXiv:2310.09191, arXiv:2310.09191 (2023).
- [42] R. Taieb, R. Dum, J. I. Cirac, P. Marte, and P. Zoller, Cooling and localization of atoms in laser-induced potential wells, *Phys. Rev. A* **49**, 4876 (1994).
- [43] C. Hölzl, A. Götzelmann, M. Wirth, M. S. Safronova, S. Weber, and F. Meinert, Motional ground-state cooling of single atoms in state-dependent optical tweezers, arXiv:2302.03940 (2023).
- [44] See Supplementary Material.
- [45] J. Sebby-Strabley, M. Anderlini, P. S. Jessen, and J. V. Porto, Lattice of double wells for manipulating pairs of cold atoms, *Phys. Rev. A* **73**, 033605 (2006).
- [46] J. T. Wilson, S. Saskin, Y. Meng, S. Ma, R. Dilip, A. P. Burgers, and J. D. Thompson, Trapping Alkaline Earth Rydberg Atoms Optical Tweezer Arrays, *Phys. Rev. Lett.* **128**, 033201 (2022).
- [47] E. Deist, J. A. Gerber, Y.-H. Lu, J. Zeiher, and D. M. Stamper-Kurn, Superresolution Microscopy of Optical Fields Using Tweezer-Trapped Single Atoms, *Phys. Rev. Lett.* **128**, 083201 (2022).
- [48] F. Gyger, M. Ammenwerth, R. Tao, H. Timme, S. Snigirev, I. Bloch, and J. Zeiher, Continuous operation of large-scale atom arrays in optical lattices, arXiv:2402.04994 (2024).
- [49] K. Slagle, Y. Liu, D. Aasen, H. Pichler, R. S. K. Mong, X. Chen, M. Endres, and J. Alicea, Quantum spin liquids bootstrapped from Ising criticality in Rydberg arrays, *Phys. Rev. B* **106**, 115122 (2022).
- [50] P. Scholl, A. L. Shaw, R. B.-S. Tsai, R. Finkelstein, J. Choi, and M. Endres, Erasure conversion in a high-fidelity Rydberg quantum simulator, arXiv:2305.03406 (2023).
- [51] L. Homeier, A. Bohrdt, S. Linsel, E. Demler, J. C. Halimeh, and F. Grusdt, Realistic scheme for quantum simulation of \mathbb{Z}_2 lattice gauge theories with dynamical matter in (2+1)D, *Communications Physics* **6**, 127 (2023).
- [52] D. Malz and J. I. Cirac, Few-Body Analog Quantum Simulation with Rydberg-Dressed Atoms in Optical Lattices, *PRX Quantum* **4**, 020301 (2023).
- [53] G. Bornet, G. Emperauger, C. Chen, B. Ye, M. Block, M. Bintz, J. A. Boyd, D. Barredo, T. Comparin, F. Mezzacapo, T. Roscilde, T. Lahaye, N. Y. Yao, and A. Browaeys, Scalable spin squeezing in a dipolar Rydberg atom array, *Nature* 10.1038/s41586-023-06414-9 (2023).
- [54] J. T. Young, S. R. Muleady, M. A. Perlin, A. M. Kaufman, and A. M. Rey, Enhancing spin squeezing using soft-core interactions, *Phys. Rev. Res.* **5**, L012033 (2023).
- [55] M. A. Norcia, J. R. K. Cline, J. P. Bartolotta, M. J. Holland, and J. K. Thompson, Narrow-line laser cooling by adiabatic transfer, *New. J. Phys.* **20**, 023021 (2018).
- [56] P. S. Salter and M. J. Booth, *Designing and aligning optical systems incorporating Liquid crystal spatial light modulators (SLMs)* (2020).
- [57] P. Zupancic, P. M. Preiss, R. Ma, A. Lukin, M. Eric Tai, M. Rispoli, R. Islam, and M. Greiner, Ultra-precise holographic beam shaping for microscopic quantum control, *Opt. Express* **24**, 13881 (2016).
- [58] D. Tsevas, Precise shaping of coherent laser beams with a liquid-crystal-on-silicon spatial light modulator (unpublished).
- [59] N. Jackson, R. Hanley, M. Hill, F. Leroux, C. Adams, and M. Jones, Number-resolved imaging of ^{88}Sr atoms in a long working distance optical tweezer, *SciPost Physics* **8**, 038 (2020).
- [60] D. Kim, A. Keesling, A. Omran, H. Levine, H. Bernien, M. Greiner, M. D. Lukin, and D. R. Englund, Large-scale uniform optical focus array generation with a phase spatial light modulator, *Opt. Lett.* **44**, 3178 (2019).